For submission to Fuel, January 2018

A Shock Tube Study of Jet Fuel Pyrolysis and Ignition at Elevated Pressures and Temperatures

Jiankun Shao, Yangye Zhu, Shengkai Wang, David F. Davidson, Ronald K. Hanson

Department of Mechanical Engineering

Stanford University, Stanford CA 94305

Abstract

The development of compact HyChem hybrid models for jet fuels requires datasets of pyrolysis product yields to constrain the model and of kinetic targets to evaluate the model. To this end, we have measured selected species time-histories during fuel pyrolysis using laser absorption, and ignition delay times using multiple methods behind reflected shock waves in a heated shock tube. Measurements were performed for three different jet fuels diluted in air or argon over a temperature range of 1000-1400 K, a pressure range of 12 to 40 atm, and equivalence ratios of 0.5 to 1. Fuel loading was measured using an IR He-Ne laser at 3391 nm; ethylene with a CO_2 gas laser at wavelengths of 10532 nm and 10674 nm; and methane with a tunable diode laser at wavelengths of 3175 nm and 3177 nm. Ignition delay times were measured in three ways: by monitoring fuel removal with laser absorption, by sidewall pressure, and by OH* emission. Particular care was taken in mixture preparation and efficient transfer of the gaseous fuel mixture to the shock tube. The current HyChem model by Wang et al. shows good agreement with these data.

Introduction

In support of the development and deployment of alternative engine fuels, recent efforts have been focused on the development of accurate and reliable chemical kinetics models for these fuels. Traditionally, a surrogate approach has been employed to facilitate the development of these models; by selecting representative hydrocarbons to mimic the real fuels; for example, primary reference fuel (PRF) and toluene reference fuel (TRF) have been used as surrogates for gasoline [1-5] and different hydrocarbon blends were used as surrogates for Jet fuel [6-9]. However, many of the proposed new alternative fuels contain species with large molecular weight and diverse compounds such as oxygenates and naphthenes whose combustion kinetics are less well known, and as such the surrogate and/or detailed reaction mechanisms for many of these alternative fuels are still in their infancy or do not exist. To exacerbate the situation, the surrogate model approach often uses a large number of fuel-related intermediate species and reactions that significantly increase the size of the surrogate mechanisms. To produce a more compact chemical kinetics model for jet fuel that accurately reproduces the pyrolysis and oxidation behavior of real jet fuel, a new approach entitled HyChem has been suggested by Wang and coworkers [10, 11]. In this approach, an experimentally constrained fuel-pyrolysis model is combined with a detailed foundational chemistry model to provide both a compact reaction mechanism and a direct link to real fuels.

In this model for large hydrocarbon oxidation, fuel molecules undergo thermal or oxidative thermal decomposition followed by oxidation of these decomposition products. At sufficiently high temperatures, the two processes are effectively separable in time or spatial scales. The model proposes that the number of significant fuel decomposition products or intermediates is

small, typically six to ten in all. The composition distribution of these rapidly-formed thermal decomposition products determines the combustion properties of the original, multi-component real fuel. At engine pyrolysis conditions, the dominant thermal decomposition product in many distillate fuels is ethylene (C_2H_4), while the smaller, but important, methane (CH_4) yields are related to the aromatic content of the original fuel [10-12]. The development of HyChem hybrid models to describe the combustion behavior of conventional and alternative fuels requires a set of kinetic targets or constraints (including methane and ethylene species time-histories) to constrain the parameters of the reaction mechanisms. These types of species time-history data for distillate fuels are scarce.

Shock tube/laser absorption methods can furnish reliable, economical and accurate kinetic targets/tests of ignition, pyrolysis and oxidation that are needed both to validate the reaction mechanisms and characterize the chemical and physical fit-for-purpose properties for these fuels. In this study, species concentration time-histories during pyrolysis using laser absorption methods provide the necessary constraint data for HyChem model generation. Ignition delay time (IDT) measurements provide separate HyChem model validation targets.

Here, three jet fuels were investigated: A1, POSF10264, a low aromatic JP-8; A2, POSF10325, an average Jet A; and A3, POSF10289, a high flash point JP-5. The U.S. Air Force POSF number identifies each particular batch of fuel. GCxGC analyses and physical properties of the fuels are given in tables in the Supplementary Material. A summary of these properties is given in Table 1 and graphic representations of the fuel composition ae shown in Figure 1.

Table 1; Properties of A1, A2, A3 fuels

					Composition (Mass %)			
Fuel	Average Formula	H/C ratio	MW (g/mol)	LHV (MJ/kg)	*n*-paraffin	*iso*-paraffin	cyclo-paraffin	aromatics
A1	$C_{10.8}H_{21.6}$	2.00	151.9	43.2	26.8	39.7	20.1	13.4
A2	$C_{11.4}H_{21.7}$	1.90	158.6	43.1	20.0	29.4	31.9	18.7
A3	$C_{12.0}H_{22.3}$	1.86	166.1	42.9	13.9	18.1	47.4	20.6

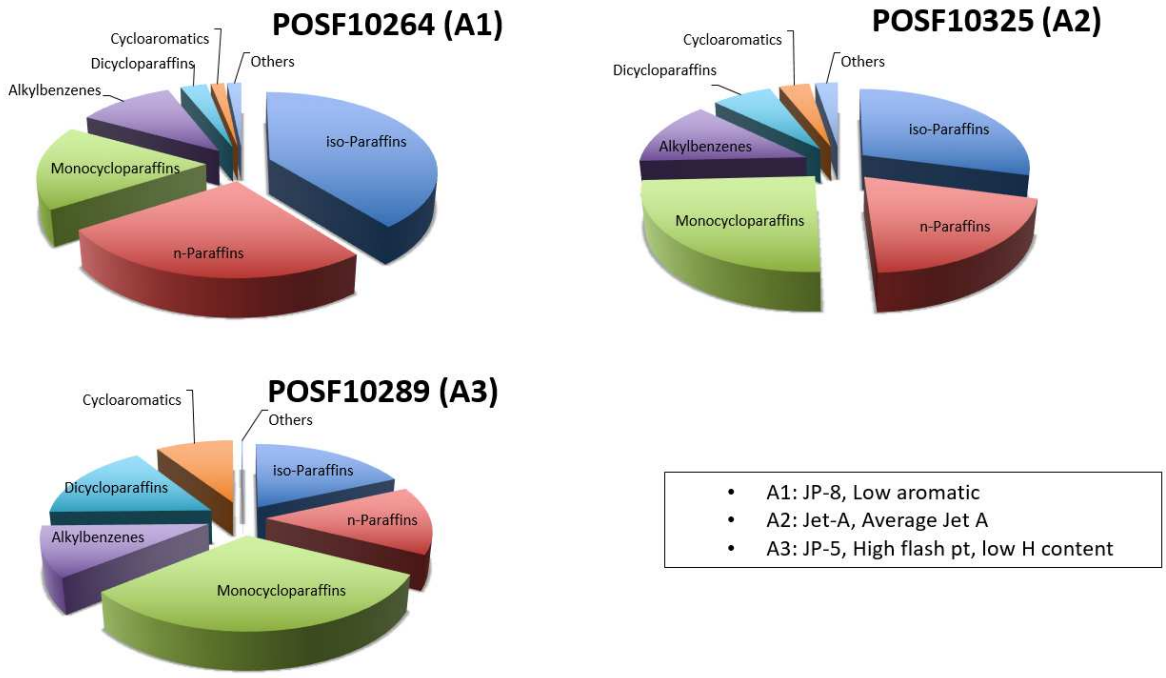

Figure 1 Components of the tested jet fuels. [11]

In this paper, experimental methods are first discussed. This is followed by experimental results and discussion for these three jet fuels. Finally, some conclusions are given. This ignition delay time and pyrolysis datasets were used in the development of the HyChem model described by

Wang and coworkers [11]. The purpose of this paper is to fully describe the measurement strategy and fully report the dataset.

Experimental method

2.1. High pressure shock tube

Current pyrolysis and ignition delay time experiments for all fuel mixtures were performed using the Stanford high-purity, high-pressure shock tube (HPST). Typical uniform test times behind reflected shock waves are of the order of 2 ms when helium is used as the driver gas. The stainless steel driven section has an internal diameter of 5 cm and was heated to 110 C to prevent condensation of the test gas mixture. Diaphragms were made of 1.27-2.0 mm thick aluminum (with cross-scribing) to allow measurements over a broad range of pressure (12 - 40 atm). Before introducing the test gas mixture, ultimate pressures in the driven section of less than 10^{-5} Torr and leak/outgassing rates of less than 10^{-4} Torr/min were achieved regularly.

The Jet fuels were obtained from the U. S. Air Force Research Laboratory. High-purity Ar and synthetic air (79% N_2/21% O_2) were supplied by Praxair as the bath gases. The liquid fuel was injected into a heated 12.8-liter stainless-steel mixing tank at 120 C. A test gas mixture of fuel/bath gas was then prepared manometrically and was stirred using a magnetically-driven vane assembly for at least 15 minutes prior to the experiments. Laser absorption at 3.39 μm was used to measure the fuel concentration in the shock tube in the test region (1.1 cm from end-wall); mixture preparing and fuel filling procedures were carefully adjusted to make sure the fuel loss ratio in the transfer to the shock tube was less than 10%. The laser absorption

measurement is necessary and essential for the accurate determination of fuel loading (needed for both accurate pyrolysis product yield ratios and accurate reflected shock test conditions) in large hydrocarbon experiments as low-vapor-pressure components of the fuel have a tendency to condense on any colder surfaces. In this study, laser absorption measurements of fuel concentration in the test region were conducted to ensure the fuel concentration uncertainty was controlled under 3%. This technique has been successfully used for the study of other distillate fuels in our laboratory, such as gasoline, diesel, and rocket fuels. [13, 14]

2.2. Shock tube diagnostics

In the current experiments, species concentrations are measured using narrow-linewidth laser absorption and the Beer-Lambert law, i.e. $-\ln((I/I_0)_\lambda) = \sigma_\lambda NL$, which relates the measured absorbance, $-\ln((I/I_0)_\lambda)$, to the unknown species mole fractions $X = NRT/P$, using the measured absorption cross sections σ_λ. The measurement of fuel loading (described in section 2.1) uses laser absorption at 3.39 μm.

Measurements of ethylene and methane time-histories use the wavelengths shown in Table 2. These measurements are affected by the simultaneous absorption by secondary or interfering species. When absorbance from one species dominated the total absorbance at a particular wavelength, and other species have broad, nearly constant, and featureless absorbance near this wavelength, a two-wavelength differential method, i.e. on-line minus off-line absorbance, can be used to determine the concentration of the dominant absorber. This is the case for ethylene, C_2H_4 [15] and methane, CH_4 [16] in this work.

Table 2: Wavelengths and laser types for some chemical kinetics target species.

Wavelength (µm)	**Laser Type**	**Usage**
3.175	Interband Cascade Laser	Methane on-line
3.177	Interband Cascade Laser	Methane off-line
3.391	He-Ne	Fuel in Region 1
10.532	CO_2	Ethylene on-line
10.675	CO_2	Ethylene off-line

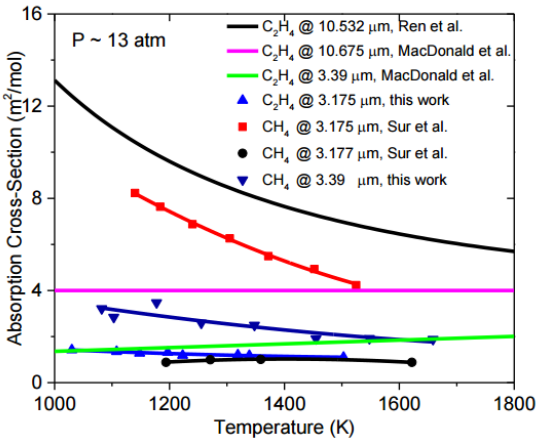

Figure 2 Representative IR absorption cross-section data.

For each wavelength, absorption cross-section data was collected for each species. Representative IR absorption cross-section data are shown in Figure 2. The measurement location of all diagnostics, including sidewall pressure, was 1.1 cm away from the end wall. Figure 3 shows a cross-section near the endwall of the test section. The left side shows a typical

set-up for ignition delay time measurement; the right side shows a typical set-up for pyrolysis laser absorption measurement. Sapphire windows were used for the signal transmissions near 3 μm and ZnSe windows were used for the signal transmissions near 10.5 μm. Pressure time-histories in the test section were monitored using a Kistler™ model 603B1 piezoelectric pressure transducer (PZT).

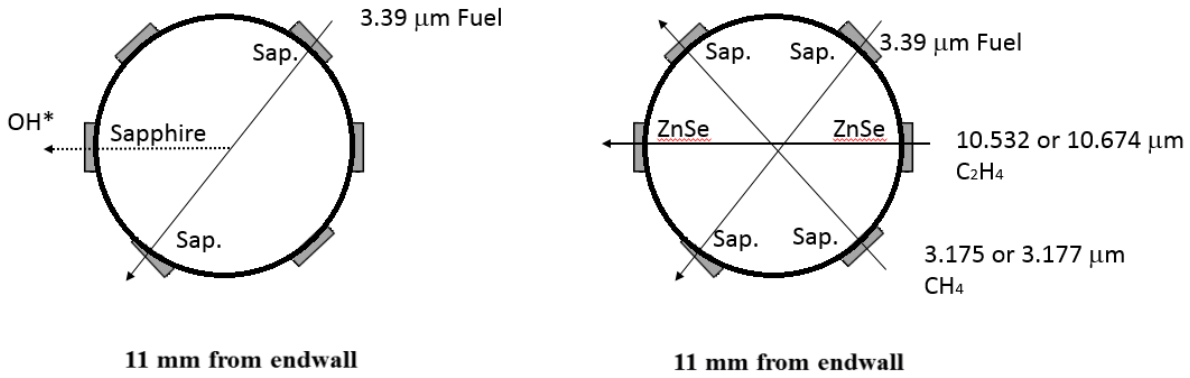

Figure 3 Diagnostics setup in the test section near the endwall.

Representative experimental data traces are shown in Figure 4; these include pressure traces, OH* emission and laser absorbance signals. The left side shows a typical plot for the pyrolysis measurement at 1293K and 12.1atm for a Jet fuel A2/Ar mixture. Methane and ethylene mole fractions were derived from the reduction of their respective online and offline laser absorbance signals. Fuel loading was determined from the 3.39 μm laser absorbance before the arrival of the incident shock wave. After the passage of the reflected shock wave, the rapid reduction in the absorbance reflects the decomposition of the major absorber, A2 fuel, during pyrolysis. The long-time plateau of the 3.39 μm laser absorbance, however, includes the absorbance of other pyrolysis products, such as methane, ethylene, and propene, as they also

absorb at this wavelength. Thus, the quantitative application of the 3.39 μm laser was only for the fuel loading experiments before the arrival of incident shock wave in this study. Ethylene and methane both begin to form when the fuel begins to decompose. This is observed by the consistency between the 3.39 μm laser absorbance decrease and methane and ethylene absorbance signal increases. The right side plot shows an oxidative case at 1031K and 11.1 atm with A2 Jet fuel/O_2/Ar, where 3.39 μm laser absorbance signal again follows the jet fuel concentration. The OH* emission near 306 nm was detected using a modified ThorLabs™ PDA36A Si detector and Schott UG5 filter with an optical setup that provided a temporal resolution of less than 7 μs. The ignition delay time was defined as the time interval between the arrival of the reflected shock and the onset of ignition determined by extrapolating the maximum slope of signals back to the baseline. All three signals, 3.39 μm laser absorption, OH* emission and pressure trace, gave consistent and nearly identical ignition delay times.

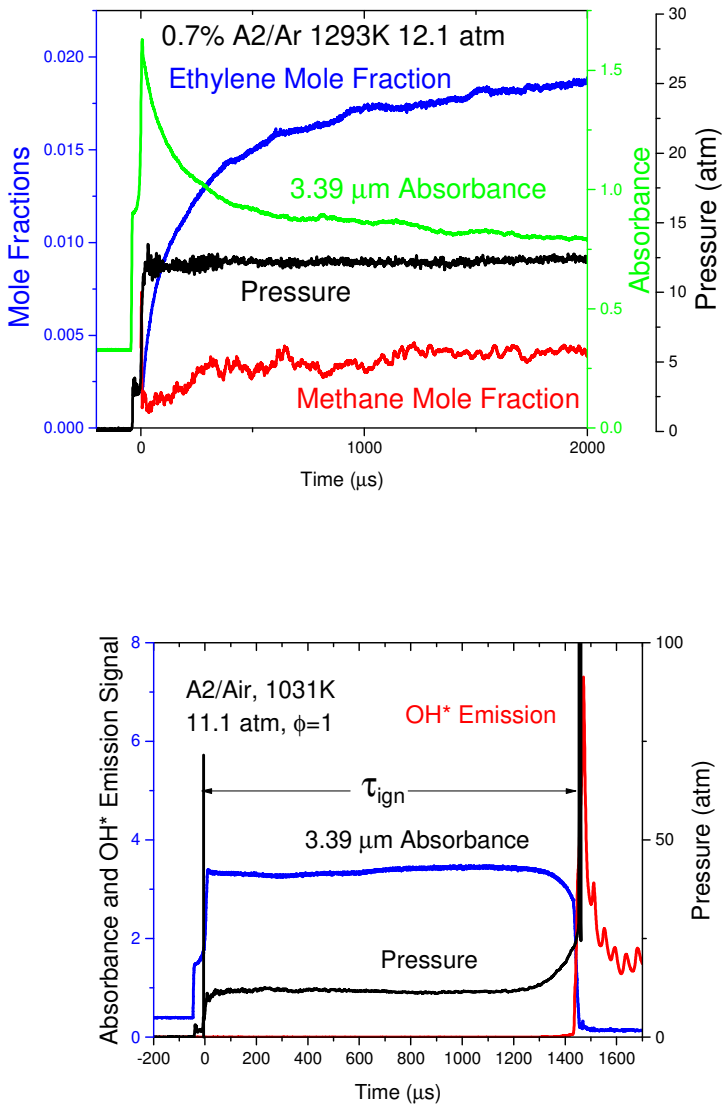

Figure 4 Example pyrolysis (top panel) and ignition delay time measurements (bottom panel) for A2. Initial reflected shock conditions for the pyrolysis experiment: 0.70% A2/argon, 1293 K, 12.1 atm; for the oxidation experiment: A2/air, ϕ = 1.0, 1031 K, 11.1 atm.

Temperatures and pressures in the current shock wave experiments are well characterized by the ideal shock relations. Accurate measurements of the incident shock speed directly translate

into accurate determinations of reflected shock temperatures and pressures. The shock arrival times in the driven section of the shock tube were recorded by five axially-spaced piezoelectric pressure transducers (PCB^{TM} 113A) located near the end-wall of the driven section. The velocity of the incident shock at the end-wall was then determined by extrapolation, allowing calculation of the initial reflected shock temperature and pressure, by using one-dimensional shock-jump relations and assuming vibrational equilibrium and frozen chemistry. Careful attention to the initial shock speed determination and fuel loading enabled reduction of the uncertainties in the initial reflected shock temperature and pressure to less than ±1%.

Results and discussions

In Section 3.1, the methane and ethylene pyrolysis speciation measurements for three jet fuel mixtures are reported. It is followed by a comparison with the current HyChem model predictions. In Section 3.2, Ignition delay time measurements for the three fuels are reported and compared with the predictions of the current HyChem model.

3.1. Pyrolysis results

Figure 5 shows representative time-history data (C_2H_4 and CH_4) for a representative reflected shock wave experiment: pyrolysis of A2 fuel in argon at 1228 K and 12.4 atm. These experiments, to our knowledge, represent the first time-resolved simultaneous measurements of C_2H_4 and CH_4 during pyrolysis of real jet fuels. Note that excellent signal-to-noise ratios (SNR) were achieved for C_2H_4, and good SNR for CH_4 was achieved, considering its weaker absorption cross section and number density product. Error bars represent ±15 and ±20% experimental uncertainties, respectively, in the C_2H_4 and CH_4 concentrations. Though the magnitudes of the

two mole fractions are dramatically different, the time-dependent shapes are similar. Both of the signals appear to rise rapidly in the early 500 μs following a near-exponential form. In addition, the measured mole fraction of CH_4 is nearly a constant fraction of the C_2H_4 mole fraction, demonstrating a near-stable branching ratio between them. These observations agree with the decomposition simulations of the HyChem model, where fuel directly decomposes into intermediate species.

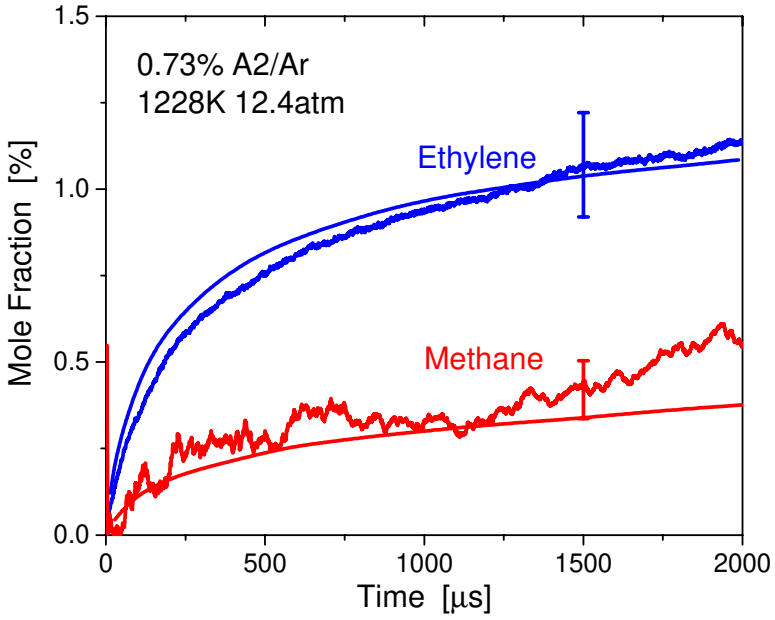

Figure 5 Laser absorption measurements of C_2H_4 and CH_4 during A2 pyrolysis. Smooth solid lines: HyChem simulations [11].

To illustrate the ethylene yield variation at different temperatures, a series of C_2H_4 mole fraction time-histories of A2/Ar mixture at different initial reflected shock temperatures are shown in Figure 6. As expected, at higher temperatures, the C_2H_4 mole fraction grows more

rapidly. This is consistent with the simulations based on HyChem or other lumped large hydrocarbon models. As expected, plateau product concentrations are different at different initial temperatures. As discussed in Ref. [11], this change in the equilibrium product concentration can be anticipated and justified based on changes in entropy of the fuel as it decomposes.

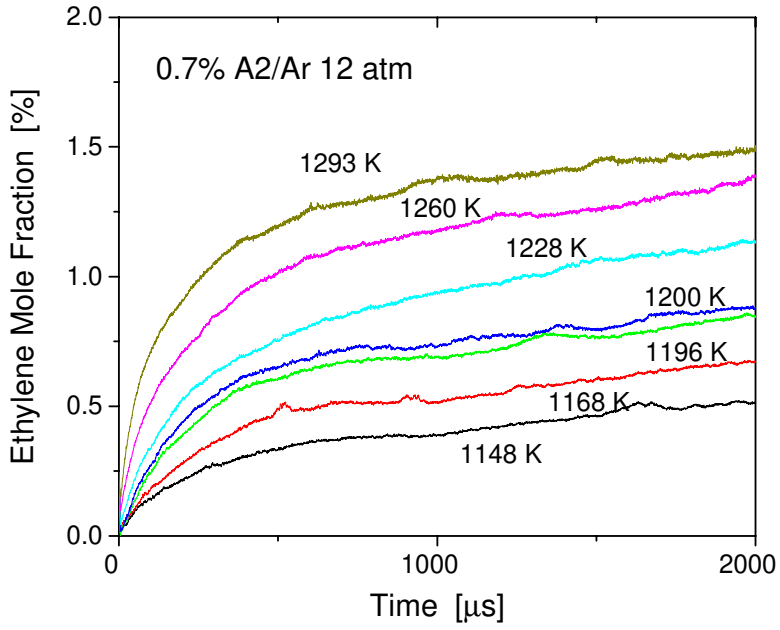

Figure 6 Ethylene time histories for 0.7% A2/argon mixtures at 12 atm.

In the following figures product yield is defined as the number of product molecules formed per equivalent initial fuel molecule. For example, if two ethylene molecule are formed during the consumption of one equivalent molecule A1 ($C_{10.8}H_{21.6}$), the ethylene yield is two. A large series of measurements similar to the ones shown in Figure 5 and Figure 6 were conducted for a range of temperatures for the three Category-A fuels at pressures near 12 atm. A summary of

the product yields, including both C_2H_4 and CH_4, at three time milestones (i.e. 0.5 ms, 1.0 ms, and 1.5 ms) are shown in Figure 7 and Table 2. The HyChem model predictions are also shown. As discussed in Ref [11], the initial parameters of the HyChem kinetic model were defined using both flow reactor and shock tube data, and thus good agreement between the HyChem model and data are expected.

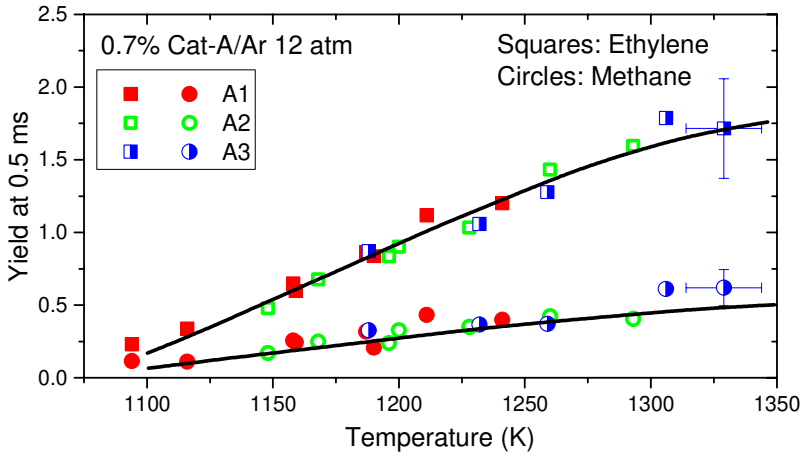

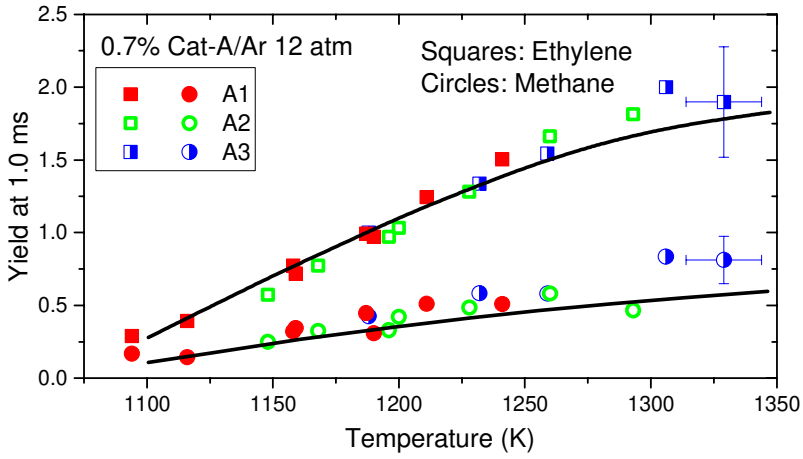

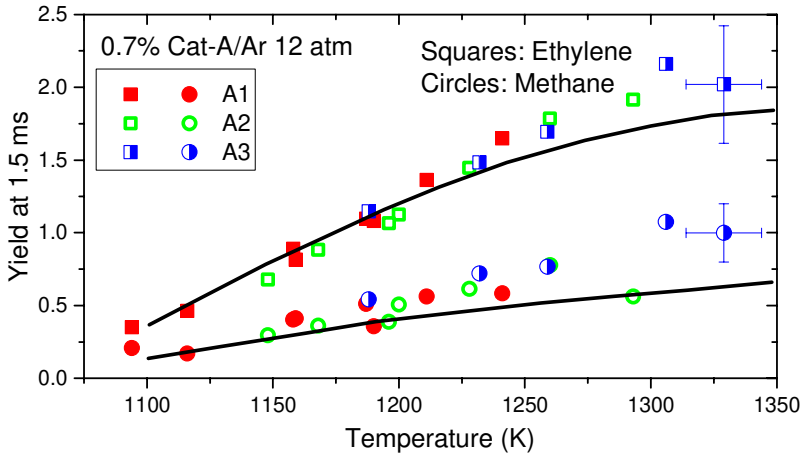

Figure 7 C_2H_4 and CH_4 yields during Category-A fuel pyrolysis at 0.5-1.5 ms. Symbols represent individual experiment. Solid lines: HyChem simulations.

Note that all three jet fuels have similar ethylene and methane yields at the similar test conditions. This observation is a direct illustration of the insensitivity of species yields to fuel composition of normal distillate fuels, as discussed earlier in the initial HyChem paper [10]. Also of note is that there is a large amount of carbon conversion to ethylene, about 30% at plateau, for all three jet fuels, which confirms ethylene as a major yield product during distillate fuel pyrolysis.

Table 2: Product yields during pyrolysis of A1, A2 and A3.

Fuel	Temperature	Pressure	Ethylene Yield	Methane Yield	Ethylene Yield	Methane Yield	Ethylene Yield	Methane Yield
%	K	atm	0.5 ms	0.5 ms	1.0 ms	1.0 ms	1.5 ms	1.5 ms
A3/Ar Mixture, 1188-1329K,12atm								
0.725	1259	12.2	1.277	0.372	1.544	0.581	1.694	0.767

0.611	1188	12.7	0.871	0.327	1.000	0.426	1.147	0.543
0.740	1329	12.0	1.715	0.620	1.898	0.813	2.020	0.999
0.589	1232	12.2	1.057	0.367	1.337	0.583	1.484	0.721
0.622	1306	11.9	1.787	0.611	2.000	0.836	2.160	1.075
A2/Ar Mixture, 1148-1293K,12atm								
0.71	1260	12.2	1.432	0.424	1.663	0.581	1.786	0.778
0.725	1200	12.5	0.902	0.328	1.032	0.422	1.125	0.507
0.727	1196	12.5	0.835	0.239	0.970	0.330	1.065	0.388
0.697	1168	12.7	0.677	0.250	0.774	0.325	0.883	0.361
0.693	1148	12.7	0.479	0.170	0.574	0.250	0.679	0.296
0.732	1228	12.4	1.034	0.350	1.281	0.486	1.445	0.614
0.750	1293	12.1	1.596	0.405	1.813	0.466	1.916	0.562
A1/Ar Mixture, 1094-1241K,12atm								
0.784	1211	12.3	1.117	0.433	1.244	0.511	1.362	0.562
0.861	1190	12.5	0.837	0.208	0.971	0.309	1.081	0.358
0.770	1187	12.4	0.863	0.317	0.993	0.447	1.097	0.512
0.602	1158	12.5	0.648	0.256	0.774	0.321	0.890	0.403
0.770	1094	13.0	0.230	0.115	0.289	0.168	0.351	0.208
0.801	1159	12.7	0.597	0.244	0.719	0.344	0.815	0.412
0.812	1116	12.9	0.338	0.112	0.393	0.144	0.463	0.170
0.799	1241	12.2	1.202	0.400	1.503	0.510	1.650	0.583

One of the basic assumptions in the HyChem approach is that the composition of the thermal decomposition products (or oxidative pyrolysis products) determines the combustion properties of the original, multi-component real fuel. Since the pyrolysis products of the three jet fuels were very similar, the overall oxidative performance, such as ignition delay time, should also be very similar also. In the following section, the optimized HyChem model [11] was used to predict the IDT.

3.2. Ignition delay time results

Figure 8 compares measured and HyChem-simulated IDT of A1, A2, and A3 fuels in 4%O_2/Ar and air bath gases. The IDT measurement results were listed in Table 3, 4 and 5. The uncertainty of the ignition delay time measured in this temperature range is ±15%. This uncertainty was estimated by the theory of propagation of uncertainty with the primary contribution from ±1% in the initial reflected-shock temperature. Overall, the HyChem simulations for the A1, A2 and A3 fuels were in reasonably good agreement with the measurements and qualitatively capture the corresponding equivalence ratio or pressure dependence of IDT.

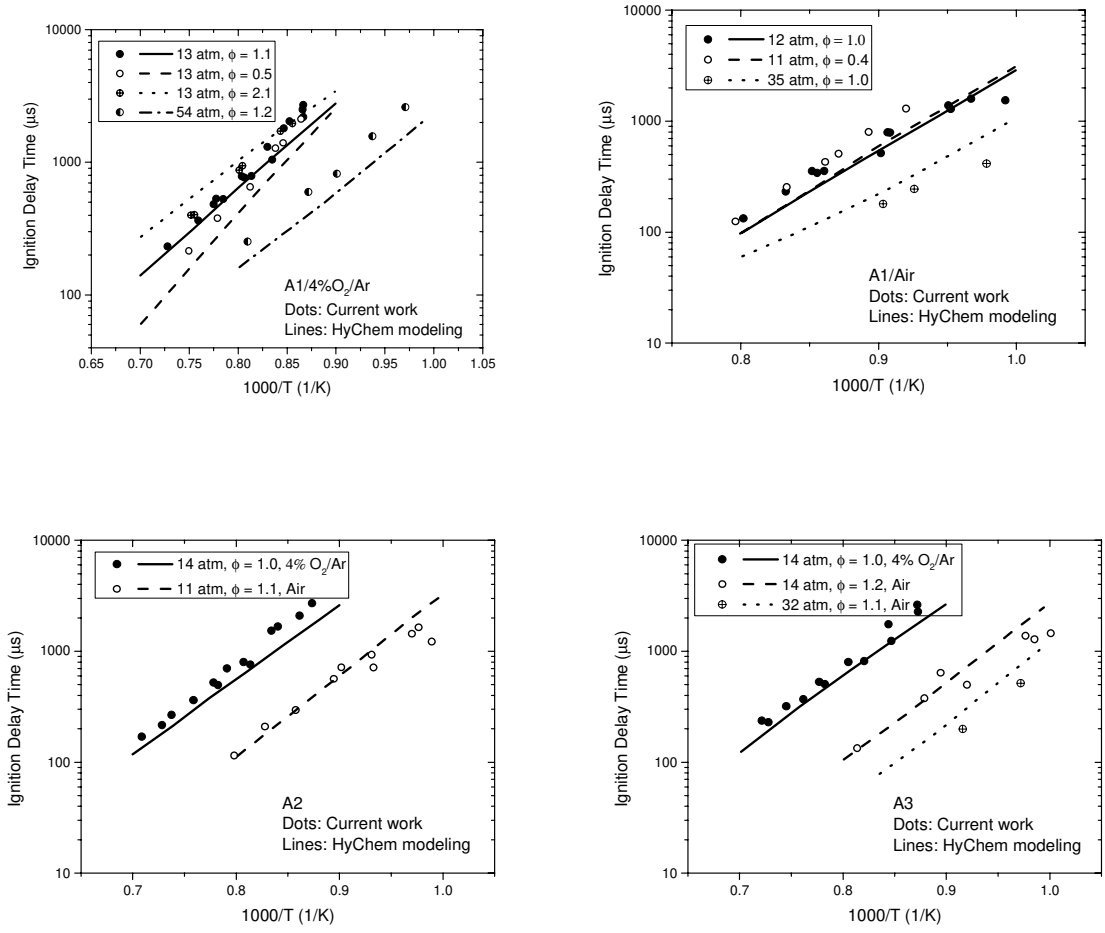

Figure 8 A1, A2 and A3 fuels in 4%O2/Ar and Air IDT data and HyChem simulations

The simulations are very consistent with the experimental measurements over a wide range of operating conditions and mixtures. In particular, the ignition delay data span a pressure range substantially wider than that of the speciation data from shock tube (~12 atm) and flow reactor (1 atm) from which the parameters of the fuel pyrolytic sub-model were derived. Note particularly that the model simulations of the IDT values at high pressures, above the pyrolysis characterization pressure range, remain in good agreement with the IDT measurements. Thus, at least in the cases studied, the HyChem model demonstrates that it can be extrapolated to

higher pressures. No lower temperature data was included in the current experiments and the simulations. However, an expanded version of the HyChem kinetic model is being developed that will include NTC region chemistry enabling the extension of this concept to lower temperatures.

There are, however, some small differences between the IDT measurements and the HyChem model worth noting. In the A1 measurements, the measured ignition delays in 4%O_2/Ar at ϕ = 2.1 appear close to those at ϕ = 1.1, while the simulations of IDT do not capture this closeness; as well, while the measured ignition delays at ϕ = 0.4 in air appear slightly longer (approximately by 15%) than those at ϕ = 1.0, the simulations did not reproduce this difference. For A2 and A3, the simulations in 4%O_2/Ar were slightly shorter (approximately by 15%) than the data. Additionally, at higher pressures, 54 atm for A1 in 4%O_2/Ar, 35 atm for A1 in air, and 32 atm for A3 in air, the disparity between data and modeling appears slightly larger (approximately by 20%) than seen in the 11 to 14 atm data. These small discrepancies between experiments and simulations may be related to details of the small species oxidation sub-mechanism, where some reaction rates constants that show high sensitivity for ignition delay time are still being improved, notably including H + O_2 +M = HO_2 +M and H + CH_3 +M = CH_4 +M reactions.

Table 3: Ignition delay time of A1 mixtures.

T(K)	P(atm)	ϕ	τign(μs)

A1/4%O2/Ar, ϕ = 1.0/0.5/2.0

1286	11.96	1.02	532
1205	12.4	1.04	1309
1244	12.26	1.05	783
1155	12.55	1.04	2498
1181	12.42	1.07	1806
1290	12.22	1.11	483
1154	12.35	1.02	2711
1240	12.66	1.01	770
1173	12.87	1.01	2039
1317	15.12	1.11	365
1374	14.80	1.02	232
1274	15.42	1.11	530
1229	15.56	1.14	790
1198	15.83	1.12	1050
1154	15.98	1.13	2200
1231	12.54	0.43	653
1193	12.65	0.49	1279
1182	12.82	0.49	1403
1157	13.00	0.50	2120
1284	12.24	0.49	379
1334	12.16	0.48	215
1186	12.59	2.14	1715
1243	12.27	2.07	942

1324	11.87	2.14	403
1169	12.40	2.11	1967
1248	12.10	2.08	873
1330	11.61	2.10	400
1110	53.80	1.25	822
1147	50.09	1.21	599
1235	49.28	1.21	253
1067	51.99	1.05	1573
1030	52.21	1.06	2613
	A1/Air, ϕ = 1.0/0.5		
1169	11.25	0.99	343
1103	11.89	0.87	793
1050	12.80	0.94	1293
1034	11.35	1.21	1593
1174	10.45	0.86	355
1162	10.54	0.96	357
1052	11.59	0.97	1385
1101	11.25	1.03	792
1201	10.57	1.02	233
1008	14.80	0.85	1545
1109	14.10	0.99	517
1247	13.00	0.97	133
1256	10.34	0.37	125
1161	11.20	0.42	430

1148	10.90	0.41	510
1087	11.42	0.40	1300
1120	11.28	0.41	800
1200	10.57	0.38	255
1107	34.11	1.06	180
1080	34.59	0.94	245
1022	35.95	1.10	415

Table 4: Ignition delay time of A2 mixtures.

T(K)	P(atm)	ϕ	τ_{ign}(μs)
	A2/4%O_2/Ar		
1239	12.81	1.03	800
1190	12.98	1.05	1673
1285	12.39	0.99	523
1145	13.16	1.05	2711
1356	12.31	1.02	267
1411	11.78	0.95	170
1264	12.65	1.00	702
1199	12.95	1.15	1535
1318	15.02	0.97	363
1373	14.76	0.93	217
1278	15.33	1.02	497
1229	15.38	1.04	760

1161	15.93	0.99	2094
	A2/Air		
1166	11.61	1.18	296
1024	12.50	0.87	1645
1109	9.86	1.11	718
1031	11.05	1.13	1440
1253	9.51	1.06	115
1208	10.24	1.07	210
1118	11.03	1.16	565
1074	11.65	0.97	930
1011	15.20	1.04	1221
1072	14.40	1.12	715

Table 5: Ignition delay time of A3 mixtures.

T(K)	P(atm)	ϕ	τ_{ign}(μs)
	A3/4%O_2/Ar		
1185	12.84	1.02	1754
1147	13.11	1.05	2623
1242	12.75	1.04	800
1287	12.44	1.02	530
1342	12.06	0.95	320
1386	11.82	0.90	237
1146	15.70	1.11	2275

1181	15.45	1.08	1240
1219	15.26	1.15	815
1278	15.17	0.94	507
1313	14.95	1.06	370
1374	14.99	1.16	230
	A3/Air		
1024	12.63	1.12	1381
1118	11.99	0.86	640
1229	10.93	1.19	134
1092	30.63	1.26	199
1029	32.36	0.91	517
999	15.30	1.19	1452
1087	14.60	1.22	498
1015	14.90	1.19	1285
1138	14.00	1.30	377

Summary

A database of pyrolysis product species time-histories and IDT measurements was generated for three Category A jet fuels. These laser absorption data were characterized by accurately known and uniform test conditions, fuel loading and species concentrations. Measured ethylene and methane product yields were found to be similar for all three Category-A fuels over temperatures from 1100 to 1350 K at 12 atm. These ethylene and methane data provided kinetic constraints for HyChem model generation. Ignition delay time data for these three fuels

at different operating conditions were also reported. The HyChem model generated based on the pyrolysis data predicts these ignition delay times consistently.

Acknowledgements

This research was supported by the Air Force Office of Scientific Research through AFOSR Grant No. FA9550-14-1-0235, with Dr. Chiping Li as contract monitor and by the US Federal Aviation Administration (FAA) Office of Environment and Energy as a part of ASCENT Project 35 under FAA Award Number: 13-C-AJFE-SU-016. Any opinions, findings, and conclusions or recommendations expressed in this material are those of the authors and do not necessarily reflect the views of the FAA or other ASCENT Sponsors.

References

1. Gauthier, B. M., Davidson, D. F., & Hanson, R. K. (2004). Shock tube determination of ignition delay times in full-blend and surrogate fuel mixtures. Combustion and Flame 139(4), 300-311.
2. Callahan, C. V., Held, T. J., Dryer, F. L., Minetti, R., Ribaucour, M., Sochet, L. R., & Rani, E. (1996). Experimental data and kinetic modeling of primary reference fuel mixtures. Proceedings of the Combustion Institute 26(1), 739-746.
3. Ra, Y., & Reitz, R. D. (2008). A reduced chemical kinetic model for IC engine combustion simulations with primary reference fuels. Combustion and Flame 155(4), 713-738.
4. Liu, Y. D., Jia, M., Xie, M. Z., & Pang, B. (2012). Enhancement on a skeletal kinetic model for primary reference fuel oxidation by using a semi-decoupling methodology. Energy and Fuels 26(12), 7069-7083.
5. Shao, J., & Rutland, C. J. (2015). Modeling investigation of different methods to suppress engine knock on a small spark ignition engine, Journal of Engineering for Gas Turbines and Power 137(6), 061506.
6. Violi, A., Yan, S., Eddings, E. G., Sarofim, A. F., Granata, S., Faravelli, T., & Ranzi, E. (2002). Experimental formulation and kinetic model for JP-8 surrogate mixtures. Combustion Science and Technology 174(11-12), 399-417.
7. Eddings, E. G., Yan, S., Ciro, W., & Sarofim, A. F. (2005). Formulation of a surrogate for the simulation of jet fuel pool fires. Combustion Science and Technology 177(4), 715-739.

8. Dooley, S., Won, S. H., Chaos, M., Heyne, J., Ju, Y., Dryer, F. L., Santoro, R. J. et al. (2010). A jet fuel surrogate formulated by real fuel properties. Combustion and Flame 157(12), 2333-2339.
9. Dooley, S., Won, S. H., Heyne, J., Farouk, T. I., Ju, Y., Dryer, F. L., Oehlschlaeger, M. A. et al. (2012). The experimental evaluation of a methodology for surrogate fuel formulation to emulate gas phase combustion kinetic phenomena. Combustion and Flame 159(4), 1444-1466.
10. Wang, H., Xu, R., Wang, K., Bowman, C. T., Hanson, R. K., Davidson, D. F., Brezinsky, C. K., Egolfopoulos, F. N., A Physics-based approach to modeling real-fuel combustion chemistry - 1 Evidence from experiments, and thermodynamic, chemical kinetic and statistical considerations (2018). In press Combustion and Flame.
11. Xu, R., Wang, K., Banerjee, S., Shao, J., Parise, T., Zhu, Y., Wang, S., Movaghar, A., Lee, D. J., Zhao, R., Han, X., Gao, Y., Lu, T., Brezinsky, K., Egolopoulos, F. N., Davidson, D. F., Hanson, R. K., Bowman, C. T., Wang, H., A Physics-based approach to modeling real-fuel combustion chemistry - 2 Reaction kinetic models of jet and rocket fuels (2018). In press Combustion and Flame.
12. Glassman, I., Yetter, R. A., Glumac, N. G. (2014). Combustion. Academic Press.
13. Davidson, D. F., Shao, J., Choudhary, R., Mehl, M., Obrecht, N., Hanson, R. K. (2018). Ignition delay time measurements and modeling for gasoline at very high pressures. Submitted to the 37th Proceedings of the Combustion Institute, November 2017.
14. Davidson, D. F., Zhu, Y., Shao, J., & Hanson, R. K. (2017). Ignition delay time correlations for distillate fuels. Fuel 187, 26-32.
15. Ren, W., Davidson, D. F., & Hanson, R. K. (2012). IR laser absorption diagnostic for C_2H_4 in shock tube kinetics studies. International Journal of Chemical Kinetics 44(6), 423-432.
16. Sur, R., Wang, S., Sun, K., Davidson, D. F., Jeffries, J. B., & Hanson, R. K. (2015). High-sensitivity interference-free diagnostic for measurement of methane in shock tubes. Journal of Quantitative Spectroscopy and Radiative Transfer 156, 80-87.

Technical Report Documentation Page

1. Report No.	2. Government Accession No.	3. Recipient's Catalog No.
j.fuel.2018.04.028		

4. Title and Subtitle	5. Report Date
A Shock Tube Study of Jet Fuel Pyrolysis and Ignition at Elevated Pressures and Temperatures	April 2018
	6. Performing Organization Code

7. Author(s)	8. Performing Organization Report No.
Jiankun Shao, Yangye Zhu, Shengkai Wang, David F. Davidson, Ronald K. Hanson	

9. Performing Organization Name and Address	10. Work Unit No. (TRAIS)
Center of Excellence for: Alternative Jet Fuels and Environment Stanford University Mechanical Engineering Department Stanford CA 94305	11. Contract or Grant No. 13-C-AFJE-SU-015

12. Sponsoring Agency Name and Address	13. Type of Report and Period Covered
Federal Aviation Administration Office of Environment and Energy	Journal Article
	14. Sponsoring Agency Code

15. Supplementary Notes

16. Abstract

The development of compact HyChem hybrid models for jet fuels requires datasets of pyrolysis product yields to constrain the model and of kinetic targets to evaluate the model. To this end, we have measured selected species time-histories during fuel pyrolysis using laser absorption, and ignition delay times using multiple methods behind reflected shock waves in a heated shock tube. Measurements were performed for three different jet fuels diluted in air or argon over a temperature range of 1000-1400 K, a pressure range of 12 to 40 atm, and equivalence ratios of 0.5 to 1. Fuel loading was measured using an IR He-Ne laser at 3391 nm; ethylene with a CO2 gas laser at wavelengths of 10532 nm and 10674 nm; and methane with a tunable diode laser at wavelengths of 3175 nm and 3177 nm. Ignition delay times were measured in three ways: by monitoring fuel removal with laser absorption, by sidewall pressure, and by OH* emission. Particular care was taken in mixture preparation and efficient transfer of the gaseous fuel mixture to the shock tube. The current HyChem model by Wang et al. shows good agreement with these data.

17. Key Words	18. Distribution Statement
Jet fuel, Shock tubes, Laser absorption, Fuel characterization, Hybrid models, ASCENT	

19. Security Classif. (of this report)	20. Security Classif. (of this page)	21. No. of Pages	22. Price
Unclassified	Unclassified		